H2020-FETOPEN-2019-01

FET-Open Challenging Current Thinking

POSEIDON

NanoPhOtonic devices applying Self-assembled colloIDs for novel ON-chip light

Starting date of the project: 01/01/2020
Duration: 48 months

= Deliverable D5.3 =

Final report on integration of light sources on-chip

Due date of deliverable: 31/12/2023
Actual submission date: 02/02/2024

WP5, Lead Beneficiary: AMO
Version: V1.0

Dissemination level		
PU	Public	X
CO	Confidential, only for members of the consortium (including the Commission Services)	
CI	Classified, information as referred to in Commission Decision 2001/844/EC	

This project has received funding from the European Union's Horizon 2020 research and innovation programme under grant agreement No 861950.

AUTHOR

Author	Organization	Contact (e-mail, phone)
Rijil Thomas	AMO GmbH	thomas@amo.de
Avinash Kumar	AMO GmbH	kumar@amo.de
Stephan Suckow	AMO GmbH	suckow@amo.de
Shu Hu	UCAM	sh2065@cam.ac.uk
Jeremy Baumberg	UCAM	jjb12@cam.ac.uk
Mario Zapata	CSIC	mzapatah@gmail.com
Rubén Esteban	CSIC	ruben_esteban@ehu.eus
Javier Aizpurua	CSIC	aizpurua@ehu.eus
Nicolas Vogel	FAU	nicolas.vogel@fau.de

DOCUMENT DATA

Keywords	Integrated photonics, light emitter, plasmonics, colloidal quantum dots
Point of Contact	Name: Dr. Rijil Thomas Partner: AMO GmbH Address: Otto-Blumenthal-Str. 25 52074 Aachen, Germany Phone: +49 2418867207 E-mail: thomas@amo.de

DISTRIBUTION LIST

Date	Issue	Recipients
10/12/2023	Draft	Partners
31/01/2024	Final draft	Partners
01/02/2024	Release candidate	Coordinator

REVIEW PROCESS

Document version	Date	Status/Change
V0.1	08/12/2023	Initial draft
V0.2	20/12/2023	WP leader review
V0.3	05/01/2024	Updated draft
V0.4	31/01/2024	Partner review
V0.5	01/02/2024	Final draft
V0.6	02/02/2024	Final version

VALIDATION PROCESS

Reviewers		Validation date
Work Package Leader	Rijil Thomas (AMO)	18/01/2024
Project Coordinator	Stephan Suckow (AMO)	25/01/2024

Executive Summary

This report includes the final concepts, simulation, and experimental results that we have achieved on the waveguide integration of colloidal emitters with metallic nanoantennae to form on-chip light sources. The focus is on emitter design, chip fabrication, emitter fabrication, and characterization of the full light source.

The results reported in deliverable D5.2 were focussing on nanoparticle on a mirror (NPoM) configurations with visible CdSe/CdS quantum dots (QDs) emitting around ~640 nm wavelength in plasmonic cavities formed by a bottom Au layer and Au nanoparticles (AuNPs). We mainly observed luminescence quenching due to the Au plane and low density of AuNPs. In the current work we are reporting on similar experiments with 10-fold higher AuNP density, leading to the demonstration of 7 to 22 times higher emission from such light sources compared to references using only similar QDs.

The focus of D5.3 are integrated plasmonic emitters with disk-on-disk (DoD) arrays, also known as double disc nanoantenna, from WP3. We have simulated and fabricated optically pumped light source chips by integrating DoD emitters into silicon nitride waveguide (WG) cavities with the same QDs. The QDs were deposited on the DoD antennae in the last step to integrate them into the plasmonic cavity between the 2 disks of the DoD configuration. This configuration achieves 20 – 40 times emission enhancement compared to the control devices. Both configurations, DoD and NPoM show clear signs of plasmonic enhancement: higher output power and efficiency, some excitation angle dependency and reduced emission lifetime are seen in agreement with the Purcell effect. The output power collected at the output waveguide facet is up to 37 pW, achieved with an estimated total system efficiency of 0.01%.

Table of contents

1. Introduction

This deliverable reports the project results and progress until M48 on the integration of colloidal emitters with the silicon nitride waveguide platform developed at AMO in collaboration with the Friedrich-Alexander-Universität (FAU), University of Cambridge (UCAM), and Consejo Superior de Investigaciones Científicas (CSIC).

It has been established that metal nanoparticles, such as spheres or nanorods, can enhance the emission of colloidal quantum dots (QDs), increasing the power of light that can be coupled to on-chip waveguides. As reported previously in D5.1, initial trials via dielectrophoresis to align gold nanorod-antennae (AuNRA) resulted in nanoparticles getting deposited randomly all over the surface. Hence to demonstrate the proof of concept we initially continued with the nanoparticle on a mirror (NPoM) approach with spherical nanoparticles for our further trials because this does not require shape alignment and is hence integration process friendly. However, since these nanoparticles are deposited in solution, there is an associated randomness which might often result in low particle count and hence a smaller number of emitters and very low output power. To mitigate this, we also investigated a second emitter configuration named disk-on-disk nanoantenna (DoD), also known as double disc nanoantenna, reported in deliverable D3.3 (WP3) into our cavities on chip. Within task T5.2 we have simulated a large landscape of nanoantenna-emitter building blocks coupled to waveguides and analyzed in more detail the configuration using the DoD. As part of task T5.3 we have optimized the integration process for the colloidal emitters and finally under task T5.4 we have performed the optical characterizations of the fabricated emitter waveguide light source structures, both with and without plasmonic enhancement.

2. Results and discussion

This report describes the methodologies and results for integrating nanoscale light sources at visible (wavelength: ~633 nm) with silicon nitride (Si_3N_4 or for brevity SiN) photonic structures. During the initial stages of the POSEIDON project, several emitter configurations were under consideration as candidates for the integration into SiN waveguides: Dimer antennae or nanorod-gap antennae (NRGA), NPoM, and decahedra-on-a-mirror (Figure 1). Among these three, the NRGA has the best potential for plasmonic enhancement, about 3-4 orders of magnitude higher than the rest, but is the most challenging to align. NPoM with spherical gold nanoparticles (AuNPs) is the most fabrication friendly approach but with the lowest plasmonic enhancement. Hence for the initial light source device we chose a NPoM configuration with spherical nanoparticles where the QDs and AuNPs were deposited and integrated by UCAM on the SiN photonic integrated circuit (PIC) fabricated by AMO. Simulations were done to verify and establish the robustness of the structure against varying the position of the emitter inside the waveguide cavity and against the process tolerances that were reported in deliverable D5.2. Then, we fabricated and characterized several of these NPoM emitter light sources. However, whereas the QDs form a self-assembled monolayer, the NPoMs are stochastically distributed, leading to low coverage of the places coupling best into the WG. To improve the intensity of the emitted light we have analysed a fourth emitter configuration called DoD (Figure 1(d)), the process for which was developed in WP3 and reported in deliverable report D3.3 by FAU. CSIC simulated the DoD configuration as well to obtain and analyse the coupling efficiency, as shown in section 2.1.

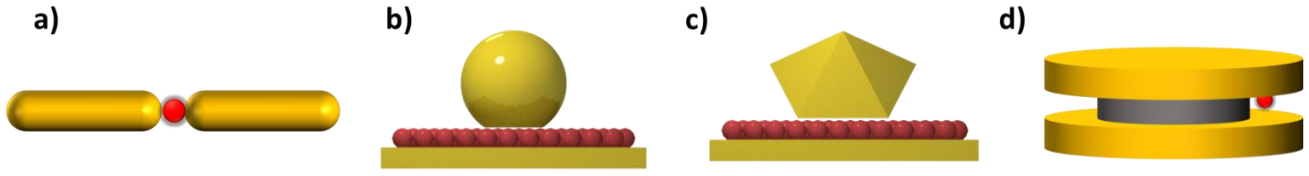

Figure 1: Emitter configurations, a) Dimer/Nanogap Antenna, b) NanoParticle on Mirror (NPoM), c) Decahedra on Mirror, d) Disk-on-Disk (DoD) antenna. Au drawn in gold, Quantum dots in red and silicon dioxide in grey.

2.1. Simulations: Nanoparticle on Mirror (NPoM) & Disk-on-Disk (DoD)

An extensive set of simulations has been performed by CSIC to characterize the light emitted by nanoantenna-emitter building blocks into a Si_3N_4 waveguides. In the previous deliverable D5.2, initial calculations were described and the dependence of the results on experimental uncertainties (small variations of the geometry or the position of the nanoantenna-emitter building block) were studied. It was shown that the results were robust to these changes.

In the present deliverable D5.3, this work is extended to i) improve the numerical accuracy, ii) simulate the behaviour of a much larger number of configurations, and iii) explore in more detail the configuration selected by the consortium. Figure 2a) shows the configuration studied in deliverable D5.2. In this case, the metallic nanoantenna consists of a spherical nanoparticle situated a few nanometres over a titanium nitride (TiN) mirror (NPoM configuration), with the QD (i.e. the emitter) situated in the gap between them. This nanoantenna-emitter building block is situated in the middle of a cavity carved in a Si_3N_4 waveguide surrounded by a dielectric cladding. The excited QD interacts with the nanoantenna, and the ensuing emitted light can be funnelled into the waveguide. This behaviour is confirmed by the field distribution of such a situation plotted in Figure 2b), which shows how light propagates along the waveguide (stronger values of $|E_y|$ along a thin rectangular region to the left and to the right of the nanoantenna-emitter block corresponding to the waveguide). All simulations were performed in the commercial COMSOL Multiphysics software, and the key parameter to be analysed is the coupling efficiency factor β, defined as

$$\beta = \frac{P_{out}}{P_0}$$

Eq (1)

In this equation, P_0 corresponds to the total power emitted by the QD, which is either radiated or absorbed by the surrounding environment and P_{out} is the power emitted into the waveguide (only the power emitted into one of the two arms of the waveguide is considered). P_{out} is calculated by integrating the power propagating along the waveguide at a given distance (e.g. 4 μm) from the input facet (the one closer to the nanoantenna-emitter building block). Thus, β indicates the proportion of the emitted photons that are funnelled into the waveguide. P_0 and P_{out} are

always calculated by treating the QD as a dipole oscillating at the emission wavelength, a treatment that is known to adequately describe the emission from a tiny emitter, except in extreme circumstances which are not considered here. An accurate analysis of β should minimize the reflections at the end of the waveguide that occurs because the simulated waveguide is long but finite. The effect of the reflection is analysed in Figure 2c), which also shows the dependence of β on the emission wavelength. The result of standard simulations with no absorption losses in the Si_3N_4 waveguide corresponds to the black line, showing clear oscillations with a periodicity that is set by the length of the waveguide. These oscillations are a consequence of reflections at the two end facets of the waveguide, producing Fabry-Pérot modes of low-quality factor in the waveguide. These oscillations can introduce a moderate error when compared to the true value for the semi-infinite waveguide. A more accurate value of β can be estimated from these simulations by taking an average, but this averaging procedure does not remove all uncertainty and it is not computationally efficient when β is required just at a few wavelengths. To circumvent these difficulties, an alternative procedure was developed consisting of adding a small amount of losses at the waveguide (in a region that is sufficiently far away from the input facet, and that does not include the plane where P_{out} is computed). The results are shown for three different distributions of losses along the waveguide (red, green, and blue lines), demonstrating the desired strong reduction of the oscillations.

In parallel to the development of this optimized procedure, the coupling efficiency factor β was calculated for a large landscape of possible configurations. Representative configurations studied are illustrated in Figure 2d). The value of β varies significantly depending on the details of the configuration, but some general conclusions can be drawn. Crucially, satisfactory coupling efficiencies β of the order of 10% are obtained for very different configurations. Further, a particularly large β is found when the nanoantenna-emitter building block is located inside the waveguide (Figure 2d, panels i and viii). However, this configuration is very challenging to fabricate, so cutting the waveguide and placing the nanoantenna-emitter building block close to the resulting input facet appears more practical and can still give satisfactorily large β (e.g. Figure 2d, panels ii and vii).

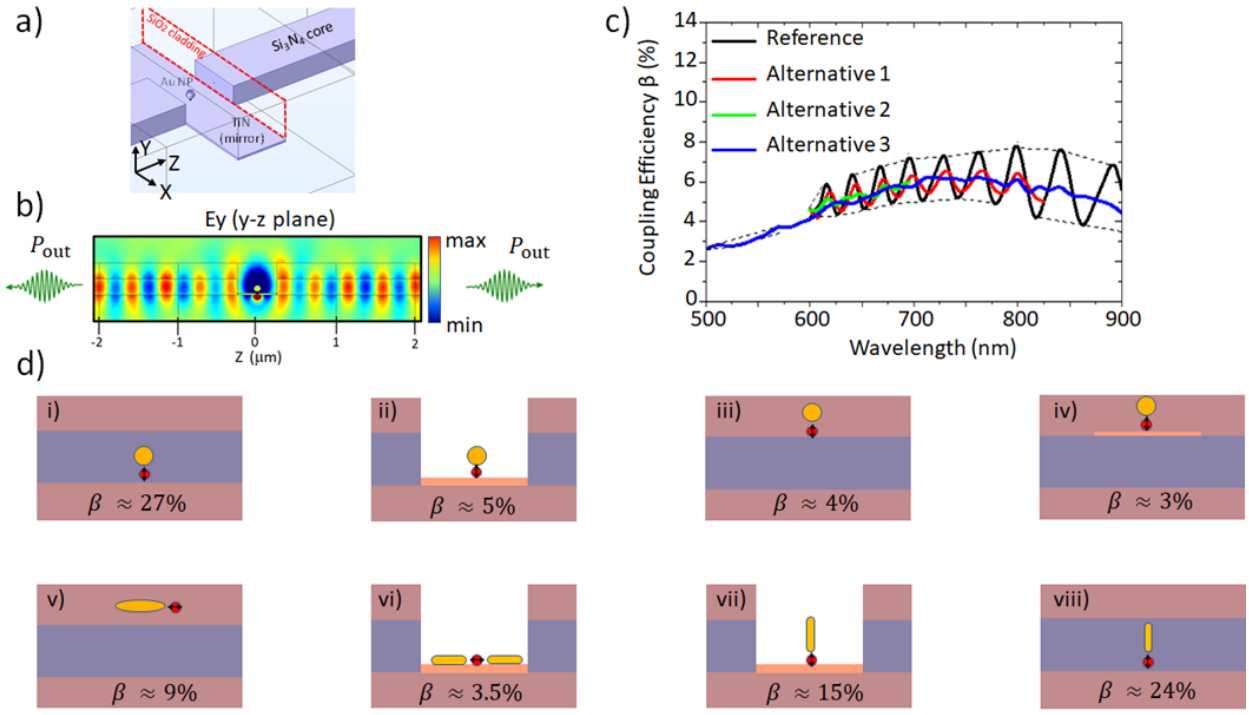

Figure 2: Emission of light from nanoantenna-emitter building blocks into waveguides. (a) Example of a geometry considered, where the emitter (QDs) is coupled to a NPoM nanoantenna (with a 40 nm radius spherical particle as the nanoparticle) and the waveguide consists of a Si_3N_4 core surrounded by a SiO_2 cladding. The width of the cavity in the waveguide (i.e. distance between the two arms of the waveguide) is 500 nm. (b) Example of the fields induced by the QD emitter situated at z=0 and coupled to the NPoM antenna in (a), showing the emission of light into the waveguide (emission to the right and to the left in the panel). (c) Coupling efficiency factor β as a function of emission wavelength, for a reference simulation with no losses in the waveguide (black line) and three alternative configurations that include some losses at the end of the waveguide to minimize the undesired reflection of the signal in the waveguide (red, green, and blue lines). (d) Schematics (not to scale) of representative configurations considered in simulations, together with the approximate value of β at the emission wavelength ≈600-650 nm. The direction of the black arrow indicates the polarization of the induced dipole at the QD (red circle). The yellow spheres and rods represent the metallic nanoantenna and the salmon slab represents the TiN mirror.

From these calculations and other results of the project, the consortium chose a particularly promising configuration, which is analysed in Figure *3*. In this case, the nanoantenna consists of two thin Au disks separated from each other by a thin dielectric spacer (DoD configuration), with the QD emitter situated in the gap between the Au disks. This nanoantenna-emitter building block is situated next to a Si_3N_4 waveguide. These calculations only include the waveguide at one side of the nanoantenna-emitter building block because, in practical experimental conditions, the other side of the waveguide is much farther away. Sketches of the DoD antenna, the waveguide, and the full system deposited in a glass substrate are shown at the top of Figure *3*a), b), and c).

The absorbance A of the nanoantennae (without QD or waveguide) is analysed first. The absorbance is defined as $A = -log(T)$, with T the transmission through the periodic system (intensity of transmitted signal normalized by incoming intensity). Figure 3a) shows the simulated absorbance spectra for different illumination angles and two types of structures. In the first one, the dielectric spacer fills up the whole gap between the metallic disks, while in the second case, the dielectric is considered to have been etched (Figure 3a, inset sketches on the right). This etching is necessary to be later able to place the QDs in the gap. The spectra are calculated for a periodic structure (Figure 3a, inset sketch bottom right) and the spectral peaks appearing are a consequence of the excitation of localized surface plasmons of the isolated nanoantennae, as well as that of grating modes induced by the periodicity of the system. The spectra of a single nanoantenna have also been calculated (not shown). The combined simulated spectra of single nanoantennae and periodic configurations enable a good understanding of the experimental situation, where a significant number of antennae in quasi-periodic structures are fabricated in the final device. Further details and experimental characterization of the response of the DoD nanoantennae can be found in deliverable D3.3.

Next, the modal structure of the infinite waveguide is characterized in Figure 3b). The dispersion relationship is plotted, where each line shows the wavevector q_z of one waveguide mode (bottom axis) as a function of the vacuum wavelength of the emitted light λ_0 (left axis). For ease of reference, the corresponding wavelength of the mode $\lambda_{mode} = 2\pi/q_z$ (top axis) and energy of the emitted photons $E_{in} = hc_0/\lambda_0$ (right axis; where h is the Planck's constant and c_0 is the speed of light in vacuum) are also indicated. The height of the Si_3N_4 is 200 nm and there is no surrounding cladding. The field distribution of the different modes is shown on the right of the dispersion relation (Figure 3b). The light emitted by the nanoantenna-emitter building block couples preferentially to the fundamental TM mode of the waveguide, TM_{00}. Even for the relatively small waveguide considered in this simulation, the two fundamental modes TM_{00} and TE_{00} are supported at the wavelengths λ_0 ≈600-700 nm that are relevant for the final device. Simulations of larger waveguides (not shown here) demonstrated the presence of more higher order modes along with these fundamental modes.

Last, the full nanoantenna-emitter-waveguide system sketched in Figure 3c) is analysed. The fields excited by the QD for emission at 650 nm are shown in Figure 3d), which again illustrates how a significant fraction of the energy is emitted into the waveguide, where it propagates over far-away distances. As described above, this funnelling of the emitted photons into the waveguide is quantified using the coupling efficiency factor. The results as a function of emission wavelength can be found in Figure 3e). Here, the power emitted into the waveguide P_{out} is obtained by integrating the power at three different planes (marked in Figure 3d, at 1 μm (black line), 2 μm (red line), and 3 μm (green line) from the waveguide input facet. The results depend on the distance relatively weakly, which verifies that the power is indeed propagating along the waveguide with minimal loss. Importantly, significant values of the coupling efficiency factor are found that is $\beta \approx 20\%$ at emission wavelength ≈600 nm. Although β drops significantly for larger wavelengths, this could be compensated by slight modifications of the waveguide geometry for emission at large wavelengths. Notably, although the exact values of β depend on the details of the geometry, the results in Figure 3e) demonstrate that large coupling efficiencies can be obtained using the DoD configuration as an emitter-nanoantenna-waveguide system, as selected by the consortium.

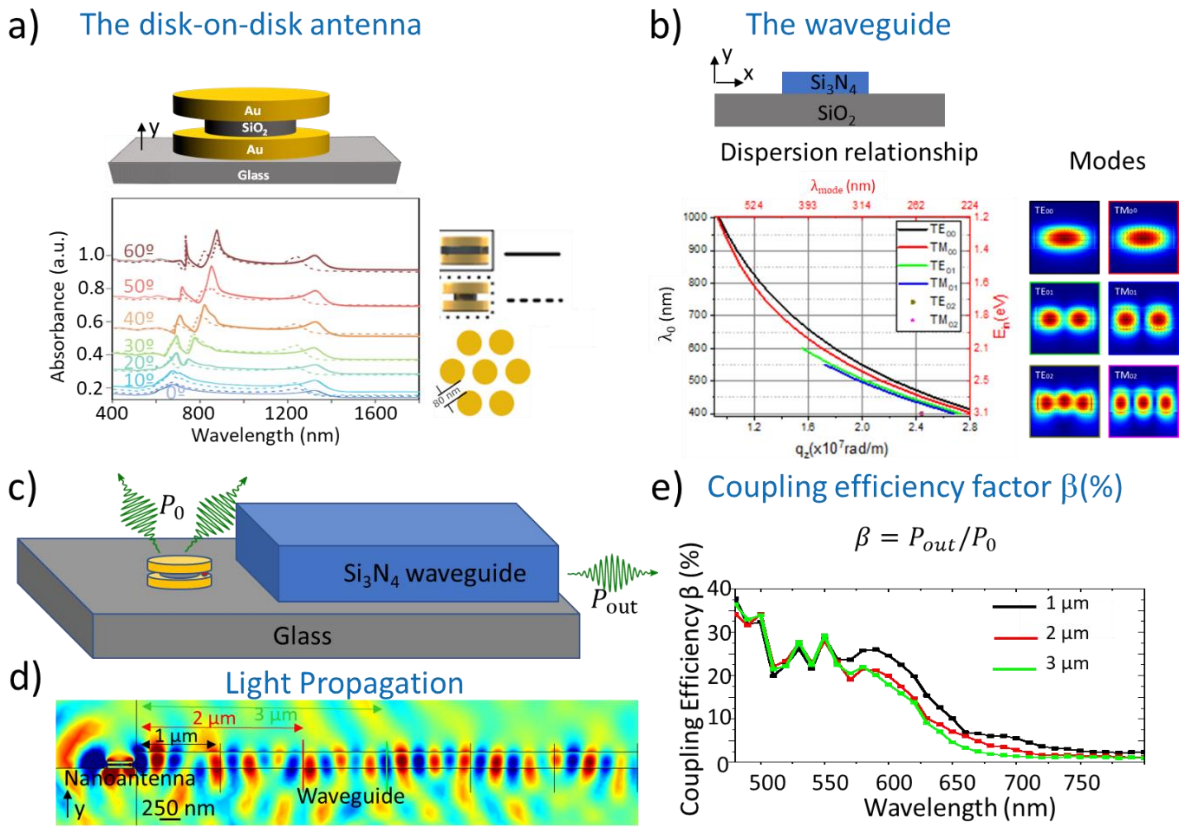

Figure 3: Light emission into a Si_3N_4 waveguide when the QD couples to a DoD nanoantenna. (a) Absorbance spectra of a periodic configuration of DoD nanoantennae, in the absence of QDs and of the waveguide, obtained as a function of the angle between the y-axis normal to the structure and the propagation direction of the plane wave that illuminates the sample. The different spectra are shifted vertically for simplicity. A sketch is shown at the top, and the periodic configuration at the bottom right side. The spectra are obtained for a structure without (solid line) or with (dashed line) etching of the SiO_2 layer separating the Au metal layers, as shown in the sketches at the centre right. (b) Characterization of the waveguide, sketched at the top. The dispersion relationship (bottom left) shows the propagating wavevector q_z along the waveguide (bottom axis; the corresponding wavelength of the induced mode, $\lambda_{mode}=2\pi/q_z$ is shown at the top axis) for different values of the vacuum wavevector λ_0 (left axis, with energy, $E_{in} \propto 1/\lambda_{mode}$ on the right axis). Each line corresponds to a mode of the waveguide, with the associated electric field distribution at a cross-section of the waveguide plotted on the right. (c) Sketch of the full system (waveguide next to a DoD nanoantenna-emitter building block). The QD emitter is represented by the small red dot between the gold disks of the nanoantenna. P_{out} corresponds to the power emitted into the waveguide, and P_0 to the total emitted power (including absorbed power). The distance from the antenna to the waveguide is 75 nm (d) Electric field distribution (real (E_y)) excited by the QD coupled to the nanoantenna (sketched on the left). The fields are funnelled into the Si_3N_4 waveguide (thin rectangle on the right). (e) Coupling efficiency factor β as a function of the emission wavelength for the configuration in (c). β is obtained by integrating the power propagating along the waveguide at three different planes, situated at 1 μm (black line), 2 μm (red line), and 3 μm (green line) from the input waveguide facet. (Sketches are not to scale.)

The effect of small changes in the configuration is illustrated next. In the experiments discussed in Section 2, the DoD can be deposited directly over the SiO_2 substrate, or over the Au metallic layer that has been deposited across the cavity. The two possibilities are sketched in Figure 4a) and d). Besides the coupling efficiency factor β, which is plotted in Figure 4c) and f), the total emitted power P_0 (solid red line) and power emitted into the waveguide P_{out} (dashed blue line) are also shown in Figure 4b) and e). The results suggest that including the Au layer affects light emission in this configuration moderately, generally increasing the total emitted power but decreasing the efficiency of the emission.

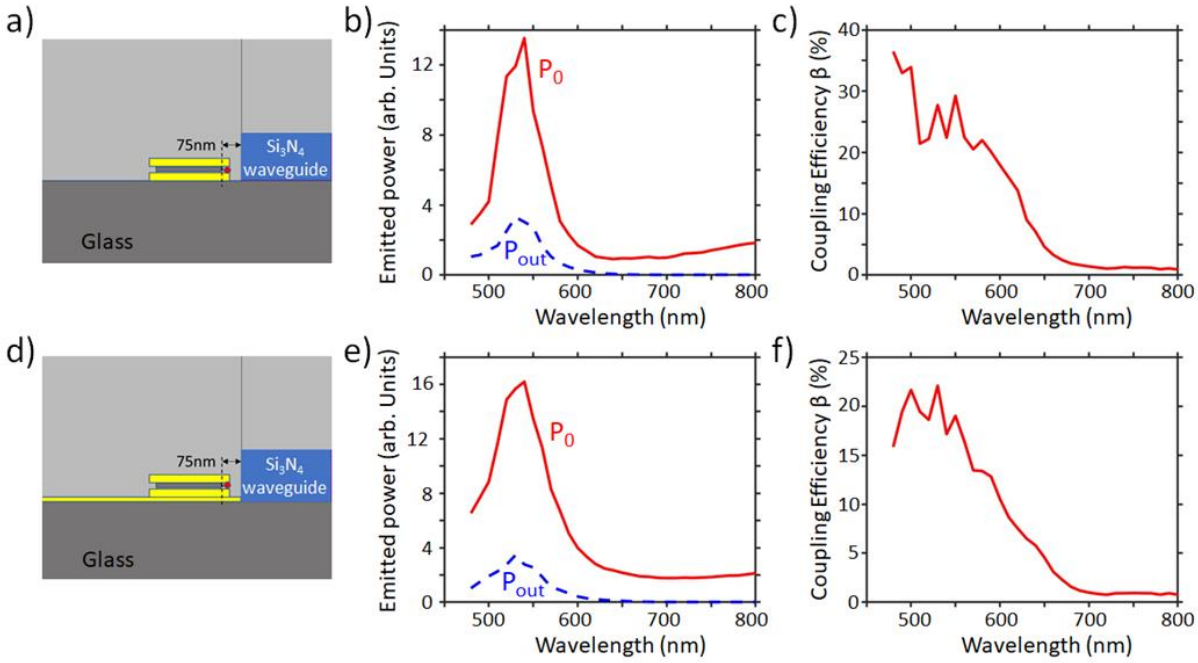

Figure 4: Effect on light emission of including an Au layer below the nanoantenna-emitter building block. (a) Sketch of the geometry considered in the absence of the gold layer, where the QD emitter (red circle) is coupled to the DoD nanoantenna (yellow metallic disks and grey spacer) placed over a glass substrate, with the resulting light emission funnelled into the Si_3N_4 waveguide (blue rectangle). (b) Total power P_0 emitted by the QD including the absorbed power (solid red line) and power P_{out} emitted into the waveguide (blue dashed line) for this system. P_{out} is calculated at a plane 3 μm away from the input facet. (c) Coupling efficiency factor $\beta = P_{out}/P_0$, for P_0 and P_{out} in (b). (d-f) Same as (a-c) but where a thin Au film is deposited between the glass substrate and the DoD nanoantenna (marked as a thin yellow film in the schematics).

Last, the effect of changing the distance between the nanoantenna-emitter building block and the waveguide is explored in Figure 5. The coupling efficiency is plotted in Figure 5b) for two different distances between the edge of the bottom disk and the waveguide facet, 70 nm and 170 nm. The increase of distance by 100 nm decreases the efficiency moderately, by about a factor 1.7 at the emission wavelength of ≈650 nm, emphasizing the interest in placing the nanoantenna-emitter building blocks as close as possible to the waveguide facet.

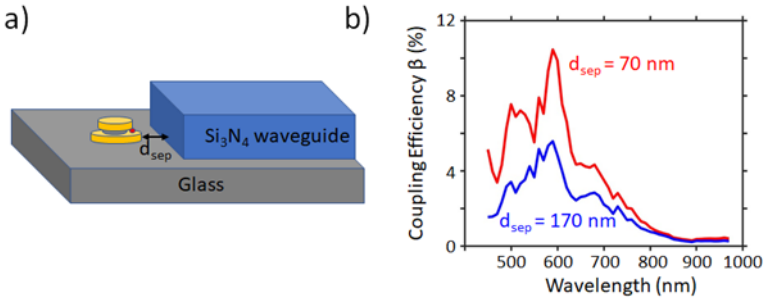

Figure 5: Effect on light emission of increasing the distance between the nanoantenna-emitter building block and the waveguide facet. (a) Sketch of geometry considered (not to scale), where the QD emitter (red circle) is coupled to the DoD nanoantenna (yellow metallic disks and grey spacer) placed over a glass substrate, with the resulting light emission funnelled into the Si_3N_4 waveguide (blue rectangle). The distance between the edge of the bottom disk and the waveguide is d_{sep}. (b) Coupling efficiency factor β as a function of the emission wavelength, for two different separation distances d_{sep}.

2.2. Fabrication and basic characterization

This section focusses on the DoD antenna configuration, as the details of NPoM fabrication have been reported before in D5.2.

2.2.1.Fabrication

In D5.1 and D5.2 we've reported on AMO's SiN test chip layout, the main fabrication process, the process optimisation of the metal gold/titanium nitride (Au/TiN) mirror deposition on SiN cavities, deposition of QDs with LOR below photoresist etc. Among the choice of bottom metal mirror Au or TiN, Au proved to be better in generating

higher output intensity than TiN in later experiments. Hence, for all the later experiments we decided to use only Au as bottom metal mirror. We followed a similar approach for DoD as of that used for NPoM. The difference is in the order in which the plasmonic structures and QDs are integrated onto the chip. Here, we first processed the DoD plasmonic structures inside the cavity (Figure 6(v)) before depositing the QDs. For the NPoM configuration, we deposited the QD layer before the AuNPs. Using the Graphic Design System (GDS) layout designed by AMO, the SiN waveguides with cavities and metal mirrors were fabricated by AMO on 6" Si wafers with 3 µm oxidized SiO2 and 200 nm Si3N4 deposited by low pressure chemical vapour deposition (LPCVD). The DoD fabrication was done by FAU and the monolayer QDs were deposited by UCAM. Figure 6 (from WP3, D3.3) shows the schematic of the process flow for the emitter (DoD + QD) integration which is explained in detail in D3.3.

In brief, a waveguide substrate is pre-structured in a way that a photoresist covers the entire substrate except for the designated deposition area within a cavity close to the waveguide (Figure 6i). Consecutive layers of Au, SiO2 and Au are deposited onto the waveguide. A layer of polystyrene particles, serving as the templating mask to form the DoD structures, is deposited onto the substrate (Figure 6iii). These spheres are reduced in size using isotropic oxygen plasma and subsequently exposed to a directed argon (Ar) etch normal to the surface, which removes all material not shielded by the templating particles (Figure 6iv). Finally, the sample is treated with an organic solvent and a basic aqueous solution to remove resist, polystyrene particles, and to open the dielectric gap separating the two gold discs (Figure 6v). Finally, a layer of colloidal QDs is deposited. Due to capillary forces, QDs are dragged into the gap opening, where they experience significant near-field enhancement (Figure 6vi).

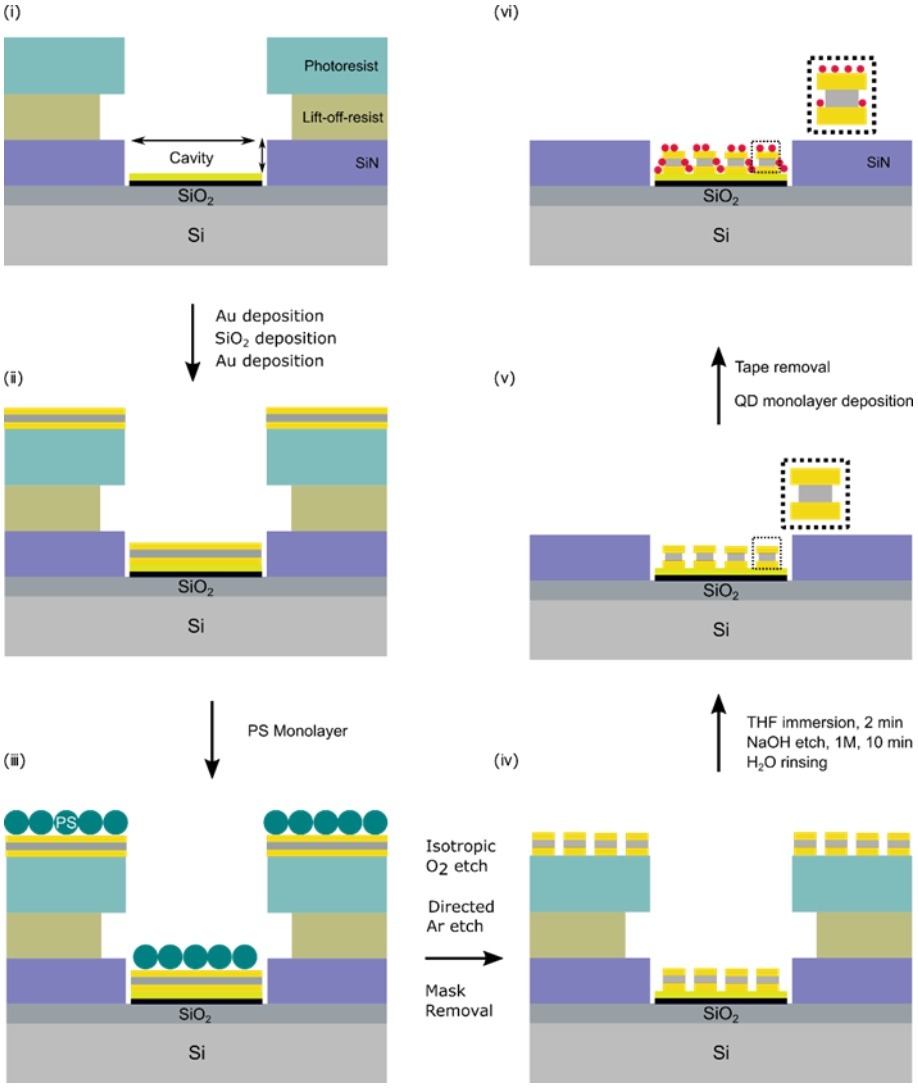

Figure 6: Fabrication of on-chip DoD nanoantenna using colloidal QDs: (i) Chip with SiN waveguide and cavity. (ii) Deposition of gold, silica, and gold layers, (iii) Monolayer assembly of polystyrene (PS) particles, (iv) Size reduction of PS particles through oxygen plasma and Ar-ion etching, resulting in DoD nanoantenna on-chip, (v) THF immersion, NaOH etching, and H_2O rinsing to achieve a reduced spacer diameter inside the cavity (boxed), (vi) Monolayer pre-assembly and placement of CdS/CdSe core-shell QDs, leading to exclusive localization within the cavity after tape removal. (from Deliverable D3.3)

Figure 7a) shows a brief schematic of the process flow for reference and Figure 7b) shows the corresponding inspection images before and after the emitter integration into the cavity. The inspection images are mainly from optical microscopy, dark field (DF) microscopy images, SEM, and photoluminescence (PL) mapping. The core shell CdSe/CdS QDs used in our experiments emit around 640 nm when excited with higher energy (wavelengths ~500 nm or lower). Hence mapping the PL around 640 nm implies mapping the QD distribution.

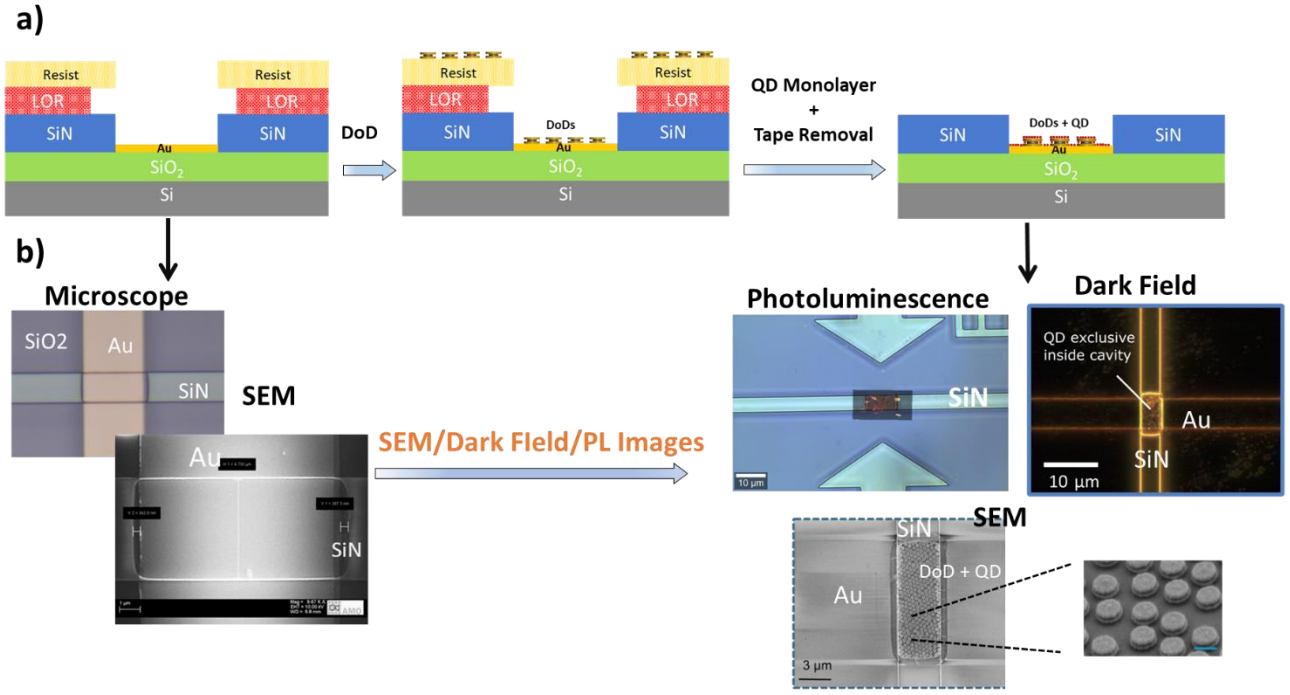

Figure 7: a) Brief schematic of the process for DoD devices with SiN waveguides with cavities, Au metal mirror, DoD structure with QDs integrated inside the waveguide cavity b) Inspection images before and after the emitter integration. Images constitute of optical microscopy, SEM, photoluminescence (PL) map and dark field images.

2.2.2. Basic characterization

The GDS design used for the characterised samples is the initial design POS01 (Figure 8 (left)). Figure 8 (right) shows the microscopic inspection images of the fabricated DoD emitter device. The microscope image of the PIC is taken after cleaving the chip through the waveguides to create waveguide facets that enable us to collect the emitted output light by a multimode fiber. The chip contains 2 different blocks for waveguide integration, named blocks D and E, with waveguides and cavities of different sizes from 0.7 µm – 5 µm wide. All cavities are of same length of 10 µm. Block D contains the cavities with Au bottom mirror across the cavities while the block E contains cavities both with and without the bottom mirror. Since the cavities in block E are placed adjacently with and without cavities, the random facet we obtain after cleaving will result in one half chip with Au metal mirror inside cavities and the other half chip without the metal mirror inside the cavities. Meanwhile the cavities from block D will always be with metal mirrors. This enables us to have both types for comparing optical performance after cleaving a chip. Figure 9 shows the SEM inspection images of a 5 µm wide cavity named D5 filled with CdSe/CdS QDs with DoD structures on the Au bottom metal mirror. SEM inspection shows a regular coverage of DoD antennae placed selectively inside the cavity after the final tape removal. We also collected photoluminescence (PL) emission spectra and performed PL mapping (Figure 10) of the QD-filled cavities using a green laser (532 nm) excitation from the top with the PL signal collected from the top as well. The PL emission peak of the QDs was confirmed to be around ~640 nm. Figure 10 top) and bottom) differ by the presence of Au metal below the DoD+QD emitters. The configuration without Au mirror (Figure 10 bottom) yields higher PL than the one with Au mirror (Figure 10 top). This difference could be attributed to the quenching of emitted light when there is a metal in the vicinity of the QDs. In both cases, the majority of the QDs happens to be outside of the DoD structures and the difference in PL observed is mainly from the behaviour of these QDs. In case of the cavity with the bottom Au metal mirror, most of the QDs outside of DoD antennas are in direct contact with the mirror which results in quenching, i.e. a reduction of PL emission. The main PL contribution originates from the QDs inside the DoD structures in between the two Au disks, where the quenching is expected to be overcompensated by the plasmonic enhancement. Moreover, since the PL is measured using an objective from the top, it could be that the directionality of the plasmonic emitter is inhibiting light from reaching the objective on the top. The light from these DoD structures preferentially radiates towards the sides of the DoD

structures, towards the waveguides and less towards the microscope objective. While this makes the optical characterization more difficult and can underestimate the PL enhancement, it is actually useful for the design of the antenna This has been reported for visible light wavelengths in the far-field emission plots in deliverable D4.1.

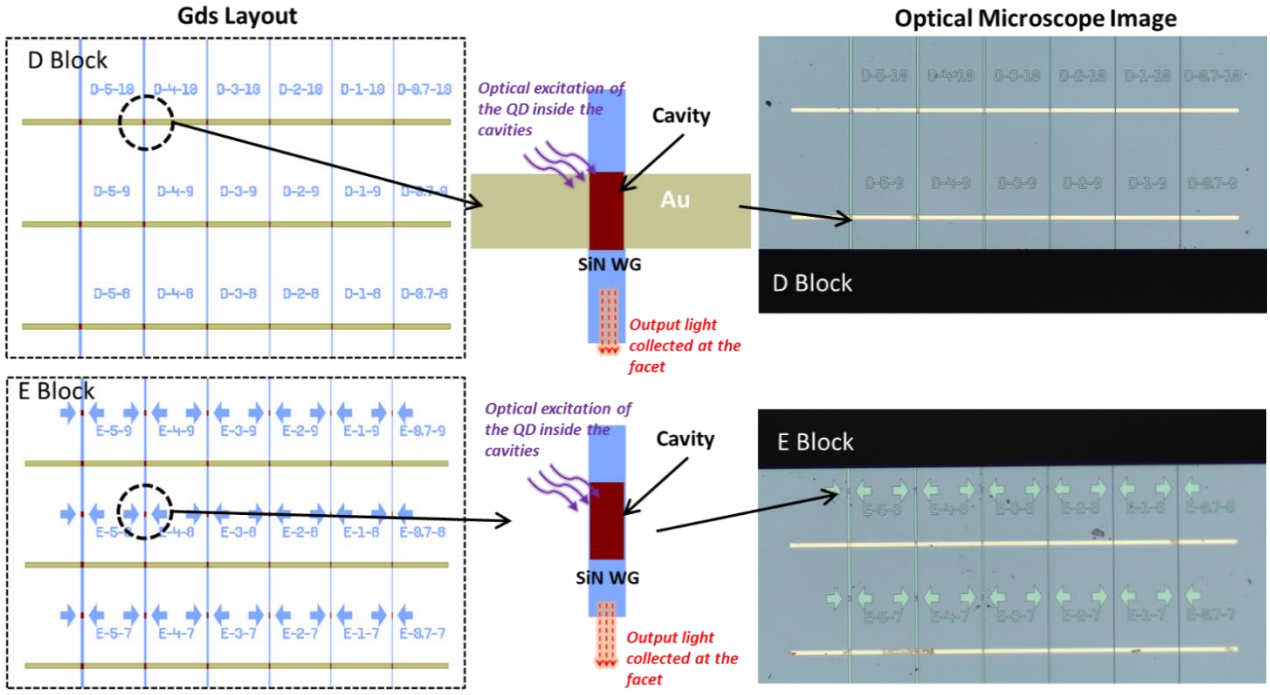

Figure 8:GDS layout (left) of block D (SiN cavities with Au bottom metal) and block E (cavities with both with and without Au bottom metal). Corresponding microscopic image (right) of the same after cleaving through the waveguide to form facets to collect emitted light.

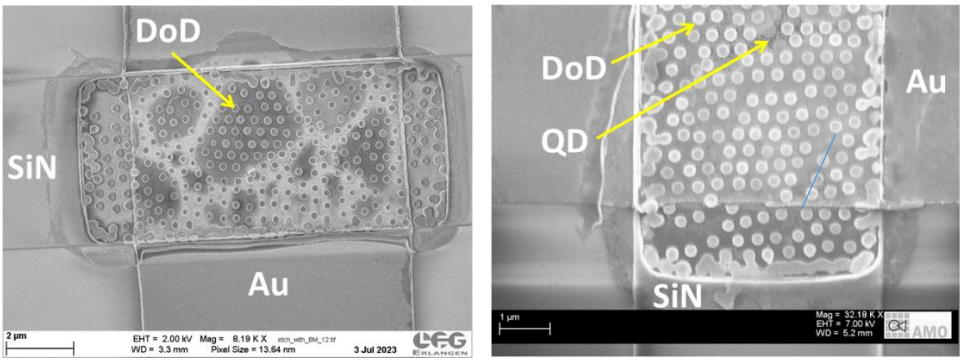

Figure 9: SEM images of QD+DoD on Au bottom metal inside SiN waveguide cavities

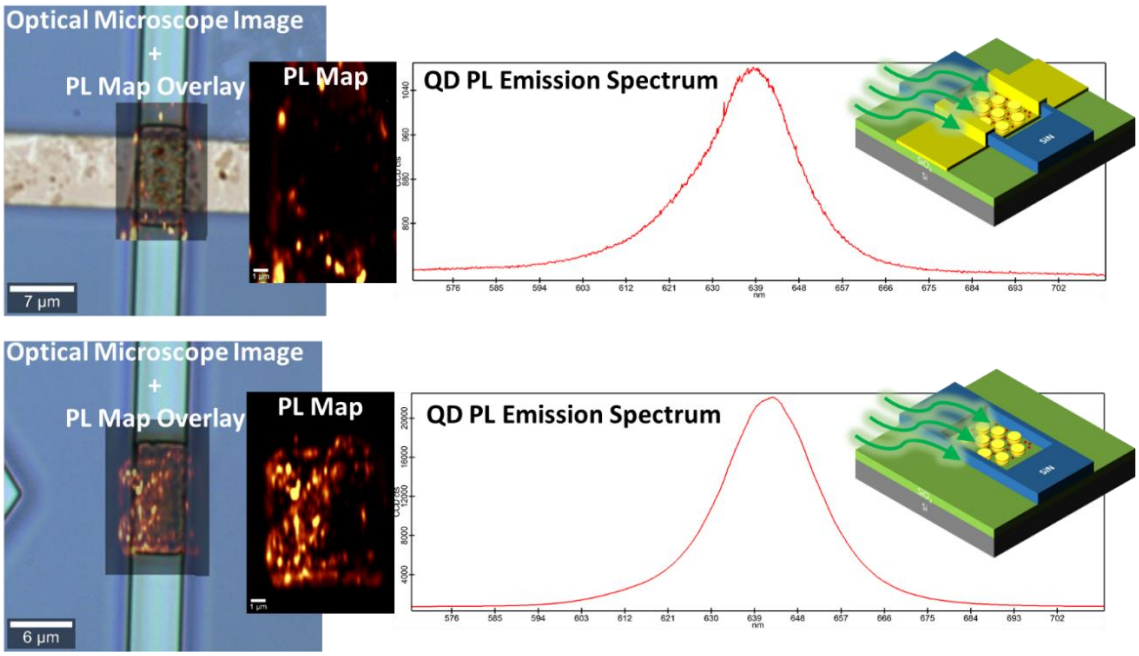

Figure 10: Photoluminescence (PL) spectra and PL mapping of QDs with (top) and without (bottom) Au metal mirror.

2.3. Optical emitter characterization

2.3.1. Setup and Methodology

The chip was mounted on a setup as shown in Figure 11. As can be seen from Figure 8, there are multiple cavities of size from 0.7 µm to 5 µm where the NPoM/DoD emitters are placed and each of these are repeated in several rows. The chip was cleaved at the face of one of these sets and then set up for edge coupling for output measurements when the emitters inside a cavity were excited from above. The excitation was done using 500 – 550 nm and 550 – 600 nm pump wavelengths filtered from a supercontinuum (SC) source with a multimode (MM) fiber with a 400 µm large core and hence a similar mode field diameter (MFD). The output at the waveguide facet was collected using a 62.5 µm MM fiber connected to a spectrometer for spectra collection, followed by a power meter with a suitable silicon detector to measure the total power in watts.

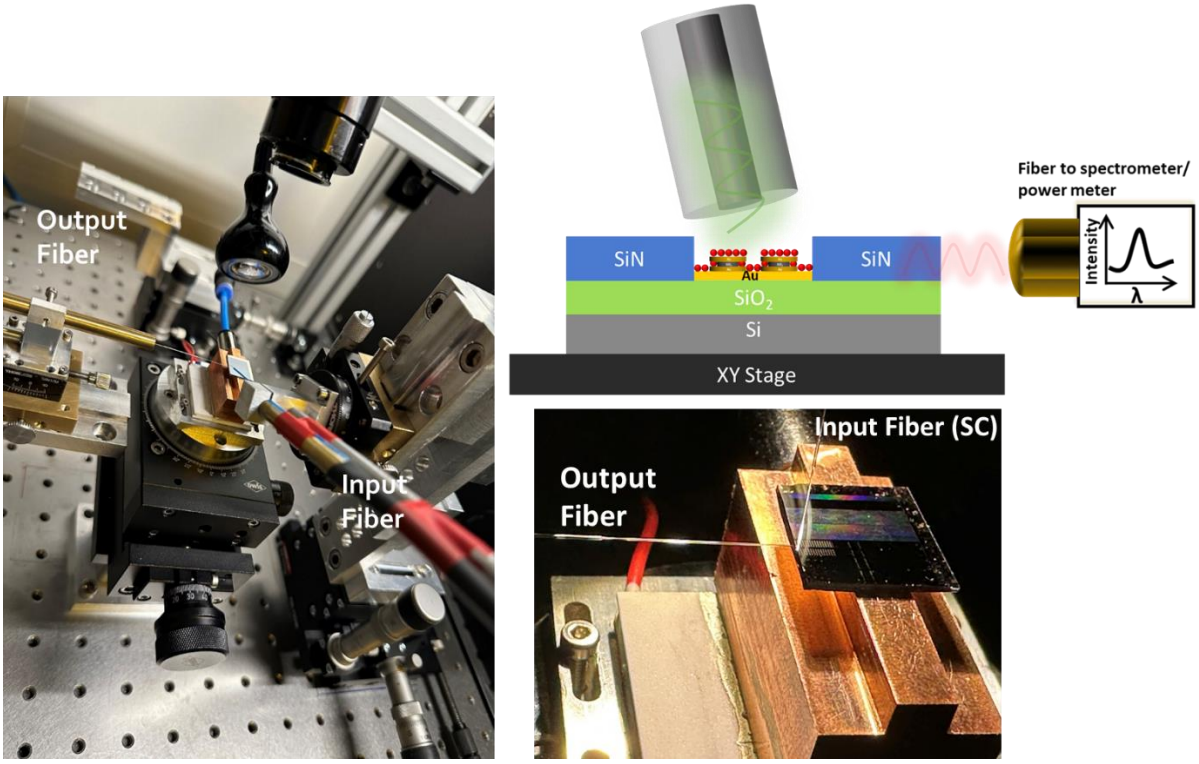

Figure 11: Excitation schematic and photos of the optical characterisation setup for waveguide integrated colloidal light sources. The large core input multimode (MM) fiber is connected to the supercontinuum laser source that is used as the pump to excite the plasmonic emitters from the top with varying angles to the surface normal. The output MM fiber is placed horizontally near the cleaved waveguide facet to collect the emitted and guided light from emitters.

Typical pump and signal spectra collected will be as shown in Figure 12. The plot shows the spectra collected in the output waveguide, i.e. scattered pump light and QD emission, depending on the angle of the pump light to the surface normal (0º - 60º) of DoD emitters inside the block D5 (block D with 5 µm wide cavity and SiN waveguide). The pump used here is 500-550 nm wavelength and the signal from the QD can be seen at ~635 nm ± 20 nm. All plots are normalised for 1 mW of input power.

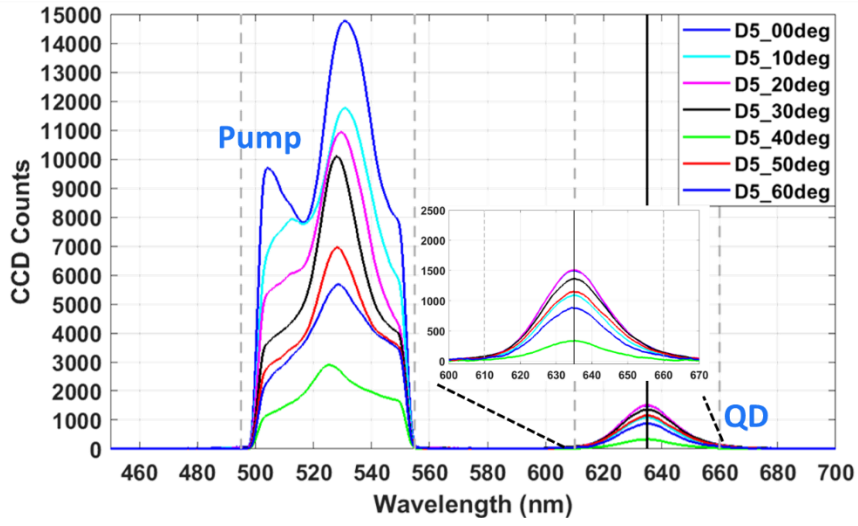

Figure 12: Pump and signal spectra collected through the output fiber from the SiN waveguide for different angles of excitation. Excitation wavelength range is 500-550 nm and the emitter block used is a DoD structure on a metal mirror from a D5 cavity. Spectra are normalised to 1 mW of input pump power.

After the spectral measurement the output power is measured using a photodetector of a known responsivity. Since the collected spectra are not single wavelengths, the power levels measured by the photodetector are not direct power values but rather the integrated power of all photons of different wavelengths hitting the detector. The measurements

therefore need to be scaled to the spectral responsivity curve of the detector, which we have measured in a separate experiment. With the knowledge of the responsivity curve of the photodetector, power measured at different responsivity or wavelengths points, and the power spectrum, the power of QD signals in the range ~635 nm ± 20 nm was estimated. Moreover, an efficiency value is calculated that represents the performance of the whole system. It is calculated as below:

$$E = \frac{S_{out}}{P_{cav}}$$

Eq (2)

where P_{cav} is the pump power received by any emitters inside the cavity area and S_{out} is the estimated power originating from the plasmonic emitters that is collected through the waveguide.

The total supercontinuum pump power is spread over the large core MM fiber, whereas only the fraction P_{cav} of power hitting the cavity and plasmonic emitters contributes to pumping the emitters. Hence only P_{cav} is considered in estimating the system efficiency. P_{cav} is found by integrating the Gaussian intensity profile coming out of the large core MM pump fiber (centered to the cavity) over the size of the cavity. Using the total input power of 1 mW in the 400 µm fiber, as measured with a power meter, only ~310 µW is received by the 5 µm wide x 10 µm long waveguide cavity. Hence, we have used this 310 µW as the input pump power for efficiency calculations of 5 µm wide cavities and correspondingly less for the smaller cavities. However, it must be pointed that not every part of the cavity area contributes to the signal collected at the end of the waveguide, but rather only few DoD structures and QD emitters placed closest to the collecting waveguide, as demonstrated exemplarily for two distances in Figure 5. This will in effect reduce the effective P_{cav} and indicates an even higher system efficiency for the emitters close to the waveguide. For example, if we assume only 1 µm active area length (out of the total 10 µm long cavity), P_{cav} is reduced to 10% and the efficiency E scales up by 1 order of magnitude. To estimate the magnitude of this effect we scanned a cavity with a 405 nm CW pump laser with a small core (~3.5 µm MFD) SM polarization maintaining fiber. The pump fiber at a 30º angle to the surface normal was first aligned in y-direction on top of the cavity by maximising the output signal strength. The fiber was then scanned along the x-direction in small steps, monitoring the output intensity at each step. The results are shown in Figure 13. However, due to the high divergence of the pump beam and probably scattered light contributions, we are hardly able to resolve the cavity. We therefore refrain from any estimations of an effective cavity size and use the full size to calculate P_{cav}.

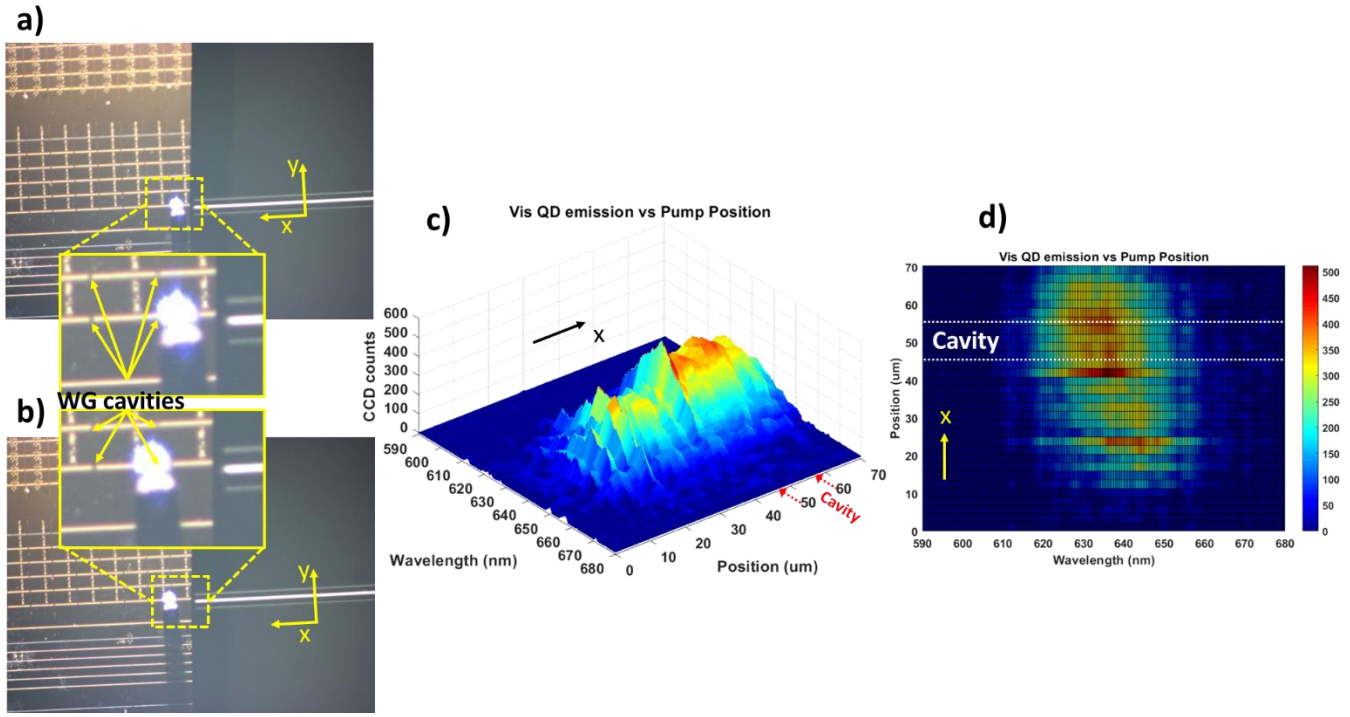

Figure 13: ***Emitter output vs pump position****. a) Microscope image of pump position placed at right where the scanning starts in x-direction; b) Microscope image of pump position placed at left end where the scanning stops in x-direction; c) 3D surface plot of the collected QD signal spectrum vs pump position; d) 2D colormap of the same data. (Note: Pump position is the center of the illuminating spot)*

2.3.2. Results

In the previous deliverable D5.2, we have reported some preliminary results measured with similar setups on collecting light emitted by QD+AuNP NPoM inside cavities. Initial measurements were done on the NPoM devices and found that the signals collected were very weak, possibly due to small number of AuNPs to form the emitters. Hence, for D5.3 we deposited AuNPs with a 10 times more concentrated solution in addition to the work on DoD emitters. Figure 14 shows a comparison of dark field imaging, indicating that the density of AuNPs inside the cavity was significantly increased.

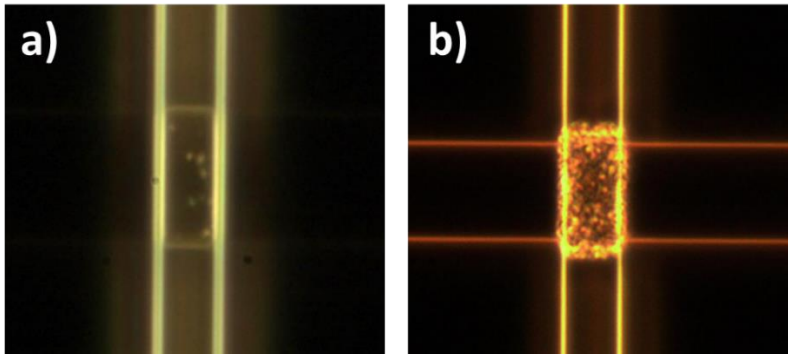

Figure 14: Dark field imaging of a Si_3N_4 waveguide cavity with NPoM structures with a) lower AuNP concentration and b) higher AuNP concentration. The difference in the brightness shows the difference in the AuNPs inside the cavity.

Figure 15 shows the comparison of signals collected from cavities with only QD as reference to that of NPoM emitters, versus the pump angle to the surface normal. Figure 15 a) shows the estimated QD power and efficiency (E_{QD}) calculated as per *Eq (2)* for only reference QDs from E5 cavities (5 µm width). The pump used here is 500 – 550 nm wavelength filtered from the supercontinuum laser. Figure 15 b) shows the estimated QD power and efficiency (E_{NPoM}) for the NPoM device from cavity D5 (5 µm width with Au mirror) and Figure 15c) shows similar results for a DoD device.

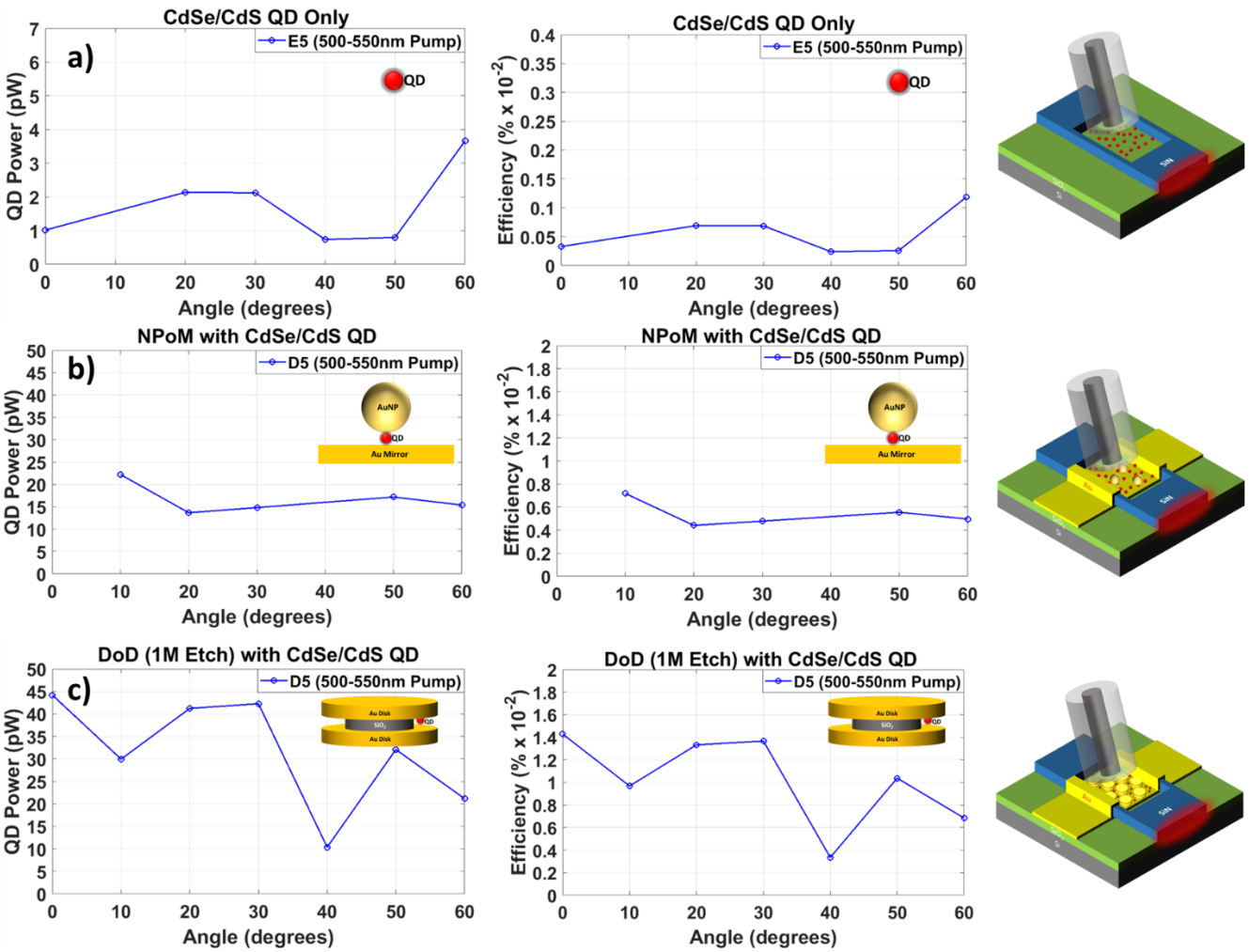

Figure 15: Comparison of estimated signal power from the emitters and final system efficiencies for a) only QD, b) NPoM, and c) DoD. (In all cases the input pump power is normalised to 310 μW received by the entire cavity.)

It should be noted that the single digit pW power estimated for only QDs (Figure 15a) has more uncertainty than the other configurations because of worse signal to noise ratio. Additionally, the DoD signal corresponding to 40° excitation (Figure 15c) could be an outlier, even though a similar trend was present in many measurements. Each configuration was excited using pump angles between 0º and 60º. Although DoD shows some dependency on the angle, the values at 0º fall out of the trend, possibly because of the ability of the pump fiber to get closer to the sample at normal incidence compared to angled configurations. It must also be pointed out that the resonant peak (>640 nm) of our fabricated DoD resonators is slightly away from the emission wavelength of the QDs (~635 ± 20 nm) and hence the excitation wavelength (500-550 nm) as well. Moreover, the NPoM resonance peak (~660 nm) is even farther from the QD emission, limiting the possible gain from the antenna. This should also result in NPoM measurements exhibiting less excitation angle dependence than DoD configurations, as there is less angle-dependent plasmonic enhancement compared to regular PL. And finally, the reference sample with only QDs is not expected to show any correlation to the pump angle as there are only QD emitters and no plasmonic antennae.

The signal collected from the 5 μm wide cavities D5 and E5 with 500 – 550 nm pump and for angles ranging from 30º to 50º, the power estimated from QDs is in the range of 1 to 2 pW, while from NPoM + QDs we collect about 16pW. This amounts to a respectable enhancement of 7 to 22. This result is especially positive, as previously we were only able to report emission quenching with the low density of NPoMs (see D5.2). Moreover, we have calculated the efficiency of 0.5×10^{-2}% using Eq (*2*) using the final output power emitted by the plasmonic antennae through the waveguide (16 pW) and input pump power received by the cavity (310 μW). Under similar conditions the power from DoD + QDs reaches ~37 pW. The corresponding enhancement for DoD devices compared to only QDs is ~20 to 40 with an efficiency of 1.2×10^{-2}%, calculated using the same equation Eq (*2*). Hence an overall 2

to 3 times higher signal was observed for DoDs compared to NPoM configurations with high particle density. The enhancement of the DoD emitters compared to just QDs is also consistent with the reduction in lifetime and Purcell factor (emission rate) enhancement measured by UHULL (Figure 16). The results labelled as Ref in Figure 16 correspond to those obtained when only QDs are present. Among the differently etched DoDs from FAU, the DoD devices used in our analysis in Figure 16 are etched with a low concentration of NaOH (0.4 M), resulting in a gap opening in the dielectric spacer of approx. 30 nm (see D3.3).

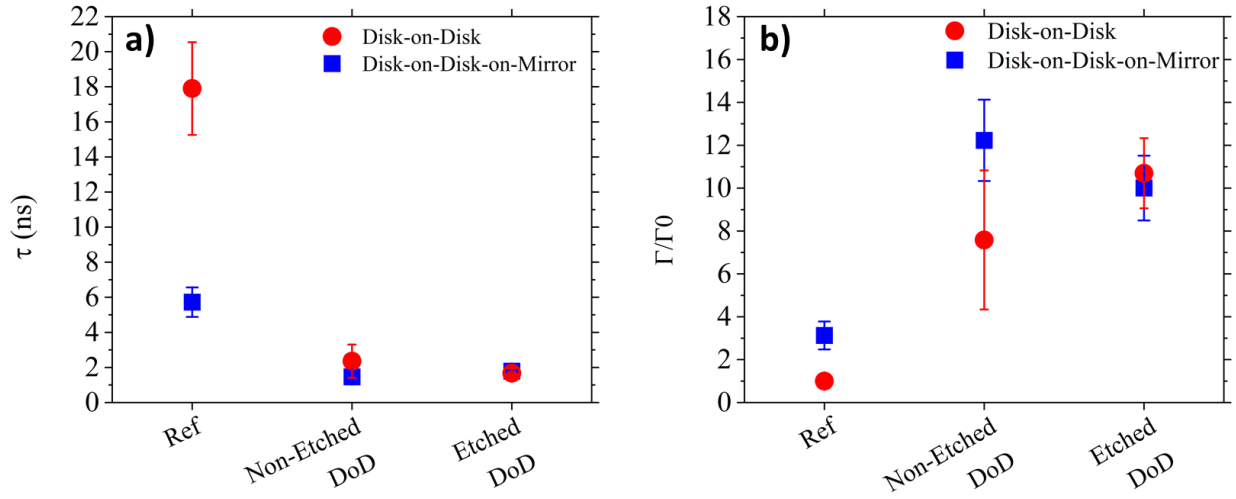

Figure 16: a) Lifetime and b) Purcell factor of QDs for 4 different configurations of only QDs, DoD with no dielectric etched, DoD with dielectric etched.

Moreover, we estimated the efficiency of the light from only QDs with analytical approximations. Below is the absorption cross-section of the QDs:

$$\sigma_{QD} = \frac{3}{2\pi}\lambda^2 \frac{\Gamma_{abs}}{\tau_{sp}} \eta_{QD}$$

Eq (3)

where σ_{QD} is the QD absorption cross-section, λ is the pump wavelength (525 nm), Γ_{abs} is the width of the experimental absorption peak (0.124 eV or 33.43 fs), τ_{sp} is the spontaneous decay lifetime (~17 ns), and η_{QD} is the quantum yield of the QDs (assumed to be 0.9). Hence the emission efficiency can be calculated as:

$$E_{QD} = \frac{\sigma_{QD}}{D_{QD}^2}$$

Eq (4)

where σ_{QD} is the QD absorption cross-section ($\sim 2.21 \times 10^{-19}\ m^2$) calculated from equation Eq (*3*) and D_{QD} is the size of the QD (~15 nm). This yields an emission efficiency of $\sim 9.83 \times 10^{-4}$. Assuming a coupling efficiency of 6% (see Figure 4f at 640 nm), the final efficiency is ~ 0.006% vs ~0.0005% measured. This difference of an order or magnitude (factor of ~12) could be due to the several differences between analytical parameters and experimental observations, especially additional losses in the experiment like worse coupling at high distances between emitter and waveguide (see Figure 5), propagation losses in the short SiN waveguide or outcoupling losses. We therefore consider the agreement between the experiment and these simulations as reasonable, supporting the presented emitter analysis.

3. Conclusions

We have shown the characterisation of 2 different plasmonically enhanced emitters, NPoM and DoD, as fully waveguide integrated optically pumped light sources on a chip as shown in Figure 15. Using the pump and QD spectra from the collected output light, photodetector measurements, and the photodetector responsivity curve, the power of the QD signal collected at the output facet is estimated and thereby the full system efficiency as described in section 2.3.1 is deduced. We used 5 μm wide "D5" cavities with bottom Au mirrors for all NPoM and DoD samples for the performance comparison. The estimated QD power from a reference sample with only QDs was in the single digit pW range. The power (efficiency) from NPoM emitters when excited at optimal angles of 30º to 50º is about 16 pW (0.5×10^{-2}%) which is ~7 to 22 times larger than that from only QD monolayers. The power (efficiency) from DoD emitters under the same conditions is about 37 pW (1.2×10^{-2}%) which is ~20 to 40 times larger than that of only QDs and almost double that of NPoM devices. It must be noted that we have assumed a uniform distribution of similar QDs with the similar quantum yield deposited inside the waveguide cavity. The excitation was also done with different angles from 0^0 - 60^0 with the expectation to demonstrate changing plasmonic response when the polarisation of the pump light better matches the electric field orientation of the plasmonic mode. Compared to the QD reference, the increase in detected DoD-QD signal power and efficiency together with the change in response to the excitation angle indicates signs of plasmonic enhancement of the emitters inside the cavity. In summary, a waveguide integrated optically pumped light source for visible wavelengths has been demonstrated and we have demonstrated plasmonic enhancement of the QD emitters by NPoM and DoD antenna configurations.

Degree of progress

We consider the Deliverable D5.3 "Final report on integration of light sources on-chip" completely fulfilled.

Dissemination level

The Deliverable D5.3 "Final report on integration of light sources on-chip" is public.